Statistical Analysis of Normal and Abnormal Dissymmetry in Volumetric Medical Images

Jean-Philippe Thirion*, Sylvain Prima, Gérard Subsol
EPIDAURE Project, INRIA
2004, route des Lucioles, BP 93
06902 Sophia Antipolis Cedex, France
[thirion][sprima][subsol]@sophia.inria.fr

Neil Roberts
MARIARC. Univ. of Liverpool
P.O Box 147. Liverpool
L69 3 BX, UNITED KINGDOM
neil@liverpool.ac.uk

Abstract

We present a general method to study the dissymmetry of anatomical structures such as the human brain. Our method relies on the estimate of 3D dissymmetry fields, the use of 3D vector field operators, and T^2 statistics to compute significance maps. We also present a fully automated implementation of this method which relies mainly on the intensive use of a 3D non-rigid inter-patient matching tool. Such a tool is applied successively between the images and their symmetric versions with respect to an arbitrary plane, both to realign the images with respect to the mid-plane of the subject and to compute a dense 3D dissymmetry map. Inter-patient matching is also used to fuse the data of a population of subjects. We then describe three main application fields: the study of the normal dissymmetry within a given population, the comparison of the dissymmetry between two populations, and the detection of the significant abnormal dissymmetries of a patient with respect to a reference population. Finally, we present preliminary results illustrating these three applications for the case of the human brain.

Keywords: Asymmetry, Dissymmetry, Brain, Medical Image Processing, Handedness

1. Introduction

The *Bauplan* or organizational scheme of many animal species is based on bilateral symmetry. Some organs appear in pairs in the body, "symmetrical" with respect to the mid-plane (limbs, eyes, ears, antennas, etc.). Other organs are placed near the mid-plane and are also approximately symmetrical (nose, tail, etc.). Such a symmetry is rather general for the human head, including the brain and its two hemispheres, but not for organs such as the liver, that has no corresponding symmetrical structure and is *asymmetrical*.

Symmetrical anatomical structures, or paired structures, are sometimes also *dissymmetrical*[1] which means that they are roughly symmetrical but each of the two organs in a pair can present a specialization and therefore a slightly different morphology. For the human brain, some normal morphological [6] and functional (described in the early work of Paul Broca) asymmetries are well known. However, due to the lack of precise morphometric tools it is still a controversial question to know to what extent functional asymmetries translate into measurable morphological dissymmetries.

The quantification of abnormal dissymmetry can also be a powerful tool to detect abnormalities. This is an alternative to the comparison of an individual to the average and standard deviation values measured in a population of normal specimens. Sometimes, the inter-individual variations in the normal population are so high (for example, brain ventricle volume variations) that they prevent a clear detection of abnormalities. In that case, comparing the relative dissymmetry measures of a patient to a population can give more relevant information than comparing absolute sizes (for example, comparing the ratio of the volumes of the two lateral ventricles instead of comparing directly the absolute ventricle volumes). However, the normal and abnormal components of the dissymmetry must still be identified in order to detect and quantify the abnormality itself. Hence population studies are also strongly needed in the analysis of the dissymmetry in a single patient to find statistically significant relative differences rather than absolute differences.

In the following, we present a new method to evaluate the normal and abnormal dissymmetry of symmetrical organs such as the human brain. Our method allows for the

*also Focus Imaging, Sophia Antipolis, France

[1] Dissymmetry (Merriam-Webster) means a deficiency of the symmetry whereas asymmetry means a lack of symmetry ("a-"= without). We make this important semantic distinction in this paper.

automatic detection of the mid-plane in the 3D images and the realignment of the image with respect to a fixed direction. We show how to compute and fuse the dissymmetry information of a population and also how to determine the regions which are significantly dissymmetrical (i.e., with respect to perfect symmetry). Then we show that the dissymmetry field of several populations can be measured and compared, and that the regions with significantly different dissymmetry can be outlined. Lastly, we present experimental results for a variety of questions such as the normal dissymmetry of human brains, the comparison of brains of left and right handed people, or the comparison of a patient presenting a focal aphasia with a normal population.

2. Existing work about dissymmetry

Asymmetry and dissymmetry have already been extensively studied in the medical field (see for example [8] for a review of some of these studies). There is for example a number of works dealing with abnormal dissymmetry of the human brain in the case of schizophrenia [9]. Here, we will not discuss the medical outcome of these studies but the geometrical aspects in these methods.

In general, the definition of homologous features between both sides of the anatomical structure is generally performed manually, which is a time consuming and tedious task, and creates a sensitivity with respect to the operator. Moreover, the geometric representations are often only based on the "lengths", or "widths", of anatomical structures viewed in projection, such as the ventricles lengths in the case of air encephalographic studies [13]. In other cases, structures are studied independently slice by slice in MR images or in cryogenic sections, with the underlying assumption that the slices are exactly perpendicular to the mid-plane, and that there is no difference in symmetry according to the axial direction.

Our method is new in that we attempt to use the geometric information present in the entire 3D image. We apply 3D elastic matching to match both sides of the object and 3D vector field analysis techniques to perform the statistical analysis. This is different from methods where segmentation tools are used independently to process both sides of the object before the two sets of shapes are finally compared. In our method, segmentation is optionally used and only at the end of the process in order to present or synthesize the dissymmetry information into a few number of parameters (for example volume variation measures of organs [19]).

There are some similarities between our work and [16]. In the latter, the mid-plane is automatically detected from the brain images using 2D snakes which are propagating through the slices to obtain a set of 2D mid-lines. A 3D plane is fitted to the set of mid-lines by a least squares technique and the 3D image is realigned with respect to it. The cortical surface is also extracted using a propagation of 2D snakes, and the perpendicular distance from the mid-plane to the cortical surface is measured for both sides, leading to a pictorial representation of the mid-plane, colored with dissymmetry values. Finally, the information of several subjects are fused, using a surface to surface matching technique based on the cortical surface.

Our method is comparable to to [16] in that the mid-plane is computed first, then the images are realigned and non-rigid matching is used to perform inter-patients data fusion. However, several other aspects are very different: we are using a volumetric matching technique instead of surface segmentation and surface matching. In particular, we determine the symmetry plane by a least squares fitting from features matched in both object sides instead of trying to detect the inter-hemispheric fissure of a brain. Our symmetry plane has therefore a different definition, much less sensitive to the flatness of the inter-hemispheric fissure and, in fact, not at all specific to brain images. Another aspect is that our dissymmetry map is defined everywhere in the 3D volume (3D image) whereas it is only defined in the mid-plane in [16] (2D image). Accordingly, inter-patients data fusion is really volumetric, allowing for local analysis of the differences. Lastly, we will see that we are able to indicate effects such as relative local expansions or atrophies, whereas only brain width differences can be measured in [16].

3. The computation of dissymmetry maps

3.1. Symmetry, chirality and mid-plane

Chirality is associated with symmetry: more precisely, two chiral objects are symmetrical with respect to a plane but *up to a rigid transform*.

For example, two hands are chiral which means that after a proper rigid placement (i.e., by joining them), they are approximately symmetrical with respect to a plane. Such anatomical structures have no symmetry plane *per se*, but we will see that their dissymmetry can be studied anyway, thanks to the 3D deformation field obtained between the image of one structure and a symmetric version of the corresponding chiral structure.

For some other structures, such as the brain, we can reasonably assume the existence of a symmetry plane that we call the *mid-plane*. As we will see, this constraint can be taken into account explicitly in the matching process that determines the correspondence between the two sides of a symmetrical object. Besides, the image of a symmetrical object can be realigned, that is, the mid-plane of this object can be placed according to a given arbitrary plane.

3.2. Automatic realignment of a symmetrical object

Our realignment method is based on the extensive use of non-rigid matching tools developed to perform 3D inter-patient matching. Examples of such tools can be found in [11, 4, 18]. For a given image I_1, we assume that the object is roughly symmetrical and that a direction approximately perpendicular to the mid-plane is known, which is a reasonable assumption for medical images such as 3D brain images. (x, y, z) being the principal axes of the 3D space, we assume for example that this is the x axis.

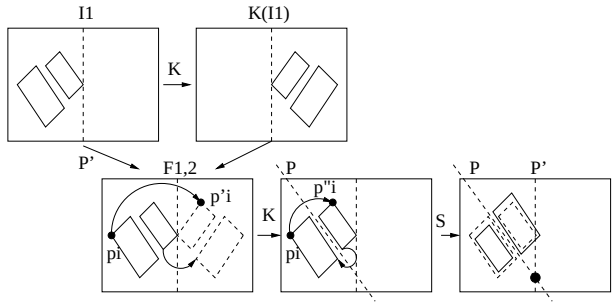

Figure 1. Basic principal of the mid-plane determination: the image I_1 is transformed into a symmetrical image $K(I_1)$ with respect to an arbitrary plane P'. Then a point to point correspondance $F_{1,2}$ is computed between both images, leading to pairs (p_i, p'_i). Applying K to the p'_i points gives couples (p_i, p''_i) of corresponding points with respect to the mid-plane P, which are used to compute the final symmetry S or equivalently the mid-plane P itself.

The first step is to choose an arbitrary plane P' in the original image to compute a chiral image $K(I_1)$ (see figure 1). If t_x is the number of voxels in the x direction, this plane can be:

$$P' : x = t_x/2 \tag{1}$$

A non-rigid technique, applied between I_1 and $K(I_1)$, gives couples $\{(p_i, p'_i)\}$ of corresponding points ($\{p_i\} \subset I_1$ and $\{p'_i\} \subset K(I_1)$). The couples $\{(p_i, p''_i))\}$ where $p''_i = K(p'_i)$ represents therefore corresponding points between both sides of the object (for example between the brain hemispheres).

The second step is to compute a symmetry S, characterized by its plane P (which means 3 parameters), that minimizes a criterion C:

$$C = \sum_i (S(p''_i) - p_i)^2 = \sum_i (S \circ K(p'_i) - p_i)^2 \tag{2}$$

It can be demonstrated (see proof in the annex) that P is going through the barycenter G of the two sets of points $\{p_i; p''_i\}$ and that its normal $\mathbf{n}$ is the eigenvector associated to the smallest eigenvalue of the following matrix I:

$$I = \sum_i (p_i - G)(p''_i - G)^\top \tag{3}$$

In particular, this plane P is not the plane which interpolates $\{p_i; p''_i\}$. If we note $R = S \circ K$, then R is an affine rotation whose rotation axis is the intersection of planes P and P'.

Determining S (3 parameters) is therefore equivalent to evaluating the affine rotation[2] R, having a rotation axis in P', that minimizes the least squares distance between $\{p_i\}$ and $\{p'_i\}$ or, in other words, that maximizes the similarity between I_1 and $K(I_1)$. This gives other practical ways to evaluate S: for example, R can be evaluated directly by using mutual information minimization techniques (see [22, 15]) adapted to affine rotations with axes in P' and applied between I_1 and $K(I_1)$. The symmetry plane P is the mid-plane of the object in I_1.

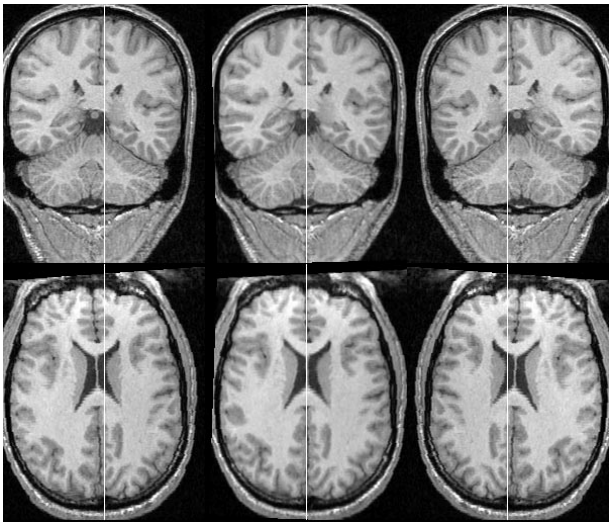

Figure 2. This image presents the result of the application of our automatic 3D realignment tool. On the left: coronal and axial view on the same patient of the original image I_1. On the right: the chiral image $K(I_1)$. On the middle: the realigned image $R^{-1/2}(I_1)$. The vertical white line is plane $P' : x = t_x/2$.

We can then demonstrate that $R^{1/2}$, the affine rotation having the same axis than R but half the rotation angle, is

[2] An affine rotation is defined by 5 parameters: the rotation axis, which is a 3D line (4 parameters) and a rotation angle. The constraint that this rotation axis has to be within a given plane P' reduces the number of free parameters to 3 only, exactly as it is the case for the symmetry S.

a rigid transform whose inverse ($R^{-1/2}$) can be used to realign the mid-plan with the arbitrary plane P' (see proof in the annex, and also figure 3). An example of realignment of a real image is shown in figure 2.

- if R is evaluated directly (image based minimization techniques), $R^{1/2}$ is conveniently determined by decomposing R into a translation $\mathbf{t}$ and a vectorial rotation represented by its rotation vector $\mathbf{r}$. The rotation in $R^{1/2}$ is then $\mathbf{r}/2$ and the translation is $(\mathbf{r}/2 + Id)^{-1}(\mathbf{t})$.
- if the symmetry plane P is evaluated directly (corresponding points techniques), it is more convenient to determine $R^{1/2}$ from the intersection of the symmetry planes P of S and P' of K, and also from the angle between these two planes.

Then a re-sampling method such as tri-linear interpolation can be applied to transform image I_1 into the realigned image $I'_1 = R^{-1/2}(I_1)$.

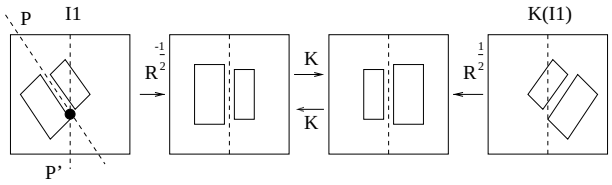

Figure 3. The transform $R^{-1/2}$, where $R = S \circ K$ and $R^{1/2} \circ R^{1/2} = R$ can be used to realign the mid-plane P with the arbitrary plane P'.

3.3. Dissymmetry field computation

A practical feature of most non-rigid inter-patient matching techniques is that the final result is sensitive to the original relative position of the two objects to match. To reduce this distance in the case of a symmetrical object, we propose to compute the dissymmetry field by applying the non-rigid matching technique between the realigned image I'_1 and its chiral version $I'_2 = K(I'_1)$ instead of directly between I_1 and $K(I_1)$.

If the objects to compare are chiral but not symmetrical (hands for example) and imaged separately (I_{left} for the left hand and I_{right} for the right hand), we propose to compute first the non-rigid correspondence between I_{left} and $K(I_{right})$. From these corresponding points, we deduce a rigid transform R by a conventional least squares method (using for example a quaternion representation of the rotations or a rotation vector representation and Kalman filtering to reject outliers, see [2]). At last we re-sample one of the two images with R: $I'_1 = R^{-1}(I_{left})$ is made superimposable to $I'_2 = K(I_{right})$ or, more symmetrically, we can re-sample both left and right images $I'_1 = R^{-1/2}(I_{left})$ and $I'_2 = R^{1/2}(K(I_{right}))$. If $R : (\mathbf{r}, \mathbf{t})$ then we have still:

$$R^{1/2} : (\mathbf{r}/2, (\mathbf{r}/2 + Id)^{-1}(\mathbf{t})) \quad (4)$$

and $R^{1/2} \circ R^{1/2} = R$. We note that we have exactly the same formulation as in the case of a symmetrical object, except that R is no longer constrained to be an affine rotation but is a general rigid displacement (6 parameters). After the realignment step, and for both cases (symmetrical or simply chiral), a *dissymmetry field* is computed between I'_1 and I'_2.

3.4. Implementation

For our experiments and for both the realignment and the dissymmetry field computation, we have used a non-rigid matching method based on "demons" (see [18]), whose output is a dense 3D deformation field $F_{1,2}$ between the two images, that is, for each voxel $p_i : (x, y, z)$ in image I'_1, we have three offsets (d_x, d_y, d_z) which give the corresponding point $p'_i : (x + d_x, y + d_y, z + d_z)$ in $K(I'_i)$. A nice feature of this algorithm is that it provides a "bijective" deformation field in the sense that it also computes an inverse deformation field $F_{2,1}$, where $F_{2,1} \circ F_{1,2}$ is very close to identity (not exactly equal because we are processing discrete vector fields).

4. The analysis of dissymmetry fields

We now discuss multiple ways to perform the analysis of dissymmetry fields. We first concentrate on the type of information which can be obtained from a single patient's image and then on how statistical analyses can be performed with respect to one or several populations.

4.1. The case of a single specimen

Several different vector field operators can be applied to a dissymmetry field in order to obtain a 3D scalar image, which can then be visualized. A simple one is the norm of the vector field $||F||$, which emphasizes indistinctly many types of dissymmetry, displaced structures as well as shearings, expansions, or atrophies.

To be more specific, dedicated operators can be used (see for example [7], [5]): for expansions or atrophies, we found in the case of temporal evolution studies of lesions that an interesting operator is $||F||div(F)$, that is, the norm times the divergence of the vector field (see [19]). The idea is that the norm characterizes the magnitude of the deformation, which holds also for large translations, while the divergence characterizes its radial aspect which can also be important in noisy regions. The feature high divergence, high magnitude is very characteristic of atrophies or expansions due,

for example, to lesions or cancer growths. Our operator gives a very high response to such phenomena. We have also developed very precise stereologic methods to evaluate quantitatively the volume variation, again for time series (also in [19]), that can be applied almost directly to the case of dissymmetry field analysis to evaluate quantitatively the relative sizes of symmetrical structures. Figure 4 presents the result of the dissymmetry field and $||F||div(F)$ operator applied to a real patient.

We have selected the region of the temporal lobes for the display (but the dissymmetry field is really 3D) because this region is very dissymmetrical in this subject (a young right handed healthy man) and, as we will see, in the majority of the subjects. In the $||F||div(F)$ image, white represents an expansion, which means a larger structure while black represents a smaller structure and grey a symmetrical structure. Hence the subject has a right temporal lobe (on the left in the image) larger than his left temporal lobe, which is a known normal dissymmetry in this population (see for example [3]). This doesn't mean that some sub-structures of the temporal lobe are not larger on the left than on the right, as it was said previously (see also [6]), but the total volume seems to be larger on the right side. Also, the dissymmetry seems to be located mainly in the white matter.

However, as stated in the introduction, one has to establish precisely the normal and abnormal components of the dissymmetry in order to provide a useful diagnosis. This means comparing a subject to a reference population. For example, we will see later on that the dissymmetry of the temporal lobes that we observe for this particular subject is confirmed to be normal thanks to a comparison with a database of 10 right handed healthy men.

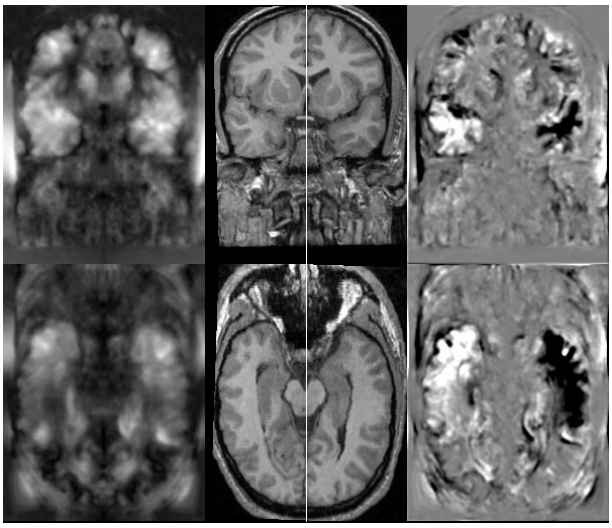

Figure 4. This figure illustrates the dissymmetry field computation (left, norm of the field) and the application of the $||F||div(F)$ operator (right) on the realigned image of a real subject (middle). Note that the dissymmetry field is a 3D image (here, only a coronal and an axial section of the same 3D image are presented).

4.2. Inter-patient fusion

Again, non-rigid inter-patient matching is used to perform data fusion between different subjects, using the same scheme as presented in [20]. A reference specimen's image I_r is chosen and realigned, and the deformation fields $F_{i,r}$ from all the realigned images I_i of specimens i to the reference image I_r are computed. The dissymmetry fields of the realigned images are then computed and an operator may be applied to this field before the result is projected onto the reference specimen's image (see figure 5). Once more, we have used the non-rigid matching method described in [18] to fuse the different specimens, and we have studied either the averaged dissymmetry vector field or the averaged result of the $||F||div(F)$ operator.

The first and second order statistical parameters are computed for each voxel of the reference image, using the projected values of the whole population (mean and variance for $||F||div(F)$, or mean and covariance matrix for F).

Finally, individual specimens or other population specimens can be projected onto the reference patient and compared with the reference population statistics to determine significant differences.

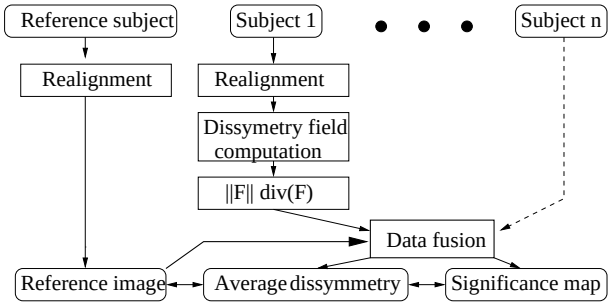

Figure 5. Fusion of the data: the images of all patients are realigned, and the dissymmetry field and norm-times-divergence operator are computed. Then all the dissymmetry maps are projected onto the realign image of a reference specimen. Lastly, the dissymmetry field and the significance map can be compared point by point to the reference image in order to determine which anatomical structure is significantly dissymmetrical.

4.3. Statistical maps and statistical tests

Different types of questions can be addressed, leading to different statistical maps and tests. The principal questions are:

- what regions in a given population are significantly dissymmetrical ?
- what regions in a given population have a significantly different dissymmetry than similar regions in another given population ?
- what regions of a given specimen are significantly different from the normal dissymmetry of a population ?

In each case, a probability map can be computed via the application of the inverse of the Fisher-Snedecor or F-function to a Mahalanobis distance or T^2-value (see for example [1, 21]). We consider here the multivariate case where the samples are random vectors of dimension p and are supposed to have a Gaussian distribution. When dealing with 3D dissymmetry fields, we have $p = 3$ and if the $||F||div(F)$ operator is used then $p = 1$ (univariate case).

4.3.1 A significant dissymmetry

The first question is typical of pure anatomical studies. The aim can be for example to designate the regions of the brain in a population of right handed young, healthy males which are significantly dissymmetrical (with respect to perfect symmetry, i.e., a null dissymmetry field). This is a classical multivariate analysis test. For a given voxel x in the reference image, the random vector for a specimen i projected in x being x_i, the average on the population of n specimens being μ and the covariance matrix being Σ, we have:

$$\begin{aligned} \mu &= \tfrac{1}{n}\textstyle\sum_{i=1}^{n} x_i \\ \Sigma &= \tfrac{1}{n-1}\textstyle\sum_{i=1}^{n}(x_i-\mu)^\top(x_i-\mu) \end{aligned} \tag{5}$$

The probability of being wrong in saying that the population has a mean different from $\mu_0 = 0$ (i.e. is different from a perfect symmetry) is called the α-value and is given by the following formula:

$$\alpha = F^{-1}_{p,n-p}\left[\frac{(n-p)}{(n-1)p}T^2(\mu_0)\right] \tag{6}$$

where:

$$T^2(\mu_0) = n(\mu-\mu_0)^\top\Sigma^{-1}(\mu-\mu_0) \tag{7}$$

The closer the α-value is to zero, the more significant the dissymmetry. The α-values computed for all voxels can be represented in a 3D image. Setting a threshold α_0 in this image (for example $\alpha_0 = 0.001$) is equivalent to performing an Hotelling's test, that is, to determining the voxels where T^2 is such that:

$$T^2 > T^2_0 = \frac{(n-1)p}{(n-p)}F_{p,n-p}(\alpha_0) \tag{8}$$

α_0 is called the significance level of the test. It is, however, unfortunate to reduce the information to only a binary image. To have a more pictorial representation of the map of α-values, we propose to display the following values: $i = \alpha_0/\alpha$ if $\alpha > \alpha_0$, $i = 1$ otherwise.

The output is a 3D image coded with floating point values where the intensity i is between 0 and 1, and saturated ($i = 1$) when the dissymmetry is highly significant. The Hotelling's test is then simply to determine the voxels $i = 1$ in such an image. In the case of expansion/contraction, the sign of the divergence can be used to provide an additional information on the nature of the dissymmetry, to lead to an image with $i \in [0, 1]$, where $i = 0$ (black) means significantly smaller (with a significance level α_0), $i = 0.5$ (gray) means undetectable dissymmetry and $i = 1.0$ (white) means significantly larger (with a significance level α_0).

4.3.2 Significant dissymmetry differences between populations

Our second question is typical of pathological studies where, other parameters being controlled, a population of n_1 pathological or atypical subjects $\{x_{1,i}\}$ with mean μ_1 is compared to a population of n_2 controls $\{x_{2,i}\}$ with mean μ_2. It can be for example a population of right handed schizophrenic males with a population of right handed healthy males. The probability of being wrong in saying that the two populations have a different mean is:

$$\alpha = F^{-1}_{p,n_1+n_2-p-1}\left[\frac{n_1+n_2-p-1}{(n_1+n_2-2)p}T^2(\mu_1,\mu_2)\right] \tag{9}$$

where:

$$T^2 = \frac{n_1 n_2}{(n_1+n_2)}(\bar{x}_2-\bar{x}_1)^\top S^{-1}(\bar{x}_2-\bar{x}_1), \tag{10}$$

$$\begin{aligned} \Sigma = \tfrac{1}{n_1+n_2-2}[&\textstyle\sum_{i=1}^{n_1}(x_{1,i}-\mu_1)^\top(x_{1,i}-\mu_1) \\ &+\textstyle\sum_{i=1}^{n_2}(x_{2,i}-\mu_2)^\top(x_{2,i}-\mu_2)] \end{aligned} \tag{11}$$

We note however that this formula is valid only under the hypothesis that the variances of the two populations of subjects (which are a-priori unknown) are exactly the same, which is not always true, especially with respect to groups of diseased patients. What statistics can tell us is that for a "reasonable" number of samples in both populations, this assumption is no longer needed. However, for reduced sets of samples and without the variance equality hypothesis, more complicated formulae have to be used (again, see [1]).

4.3.3 Significant atypical dissymmetry

Our third question can be used for individual diagnosis. A typical question might be to detect automatically a brain tumor as being a region significantly more dissymmetrical than the same region in a normal population. The probability of being wrong in saying that a value x_0 is significantly

different from a population having a mean μ and a covariance matrix Σ is a simplification of the preceding formula for $n_2 = 1$:

$$F^{-1}_{p,n-p}\left[\frac{n-p}{(n-1)p}T^2(\mu)\right] \quad (12)$$

where:

$$T^2(\mu) = \frac{n}{n+1}(\mu - x_0)^\top \Sigma^{-1}(\mu - x_0) \quad (13)$$

4.3.4 Partial conclusions about dissymmetry maps

Many combinations are possible, such as: is my patient closer to a group of epileptics than to a group of controls.... The computations which have been presented here are valid for voxel to voxel uncorrelated measurements, which unfortunately is not the case in practice because the deformation field between the direct and chiral images is regularized. However, the spatial coherency can be used to derive more robust statistical parameters, as proposed by the theory of random fields and implemented in the SPM method in the case of the analysis of functional images (for example, see [10]). We have not yet investigated the possibilities of such a method in the case of dissymmetry studies; this appears to be an interesting perspective to explore.

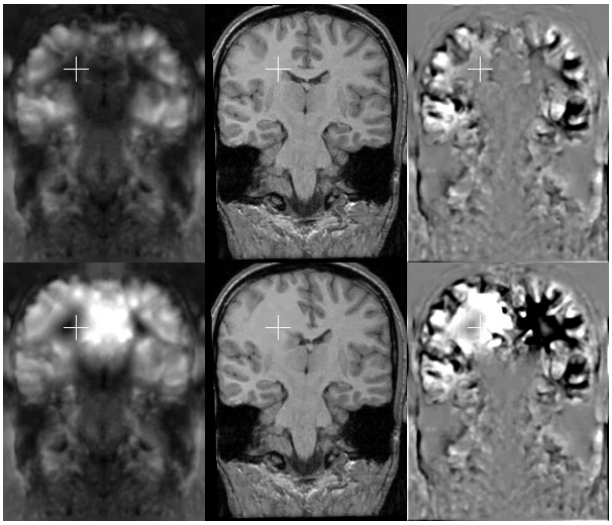

Figure 6. Synthesized expansion in 3D within the brain of an healthy subject (upper: without expansion, lower: with expansion). Middle: intensity images, left: $||F||$ and right $||F||div(F)$. The crossbars represent the focal point of the expansion.

5. Synthetic experiments

We have performed various tests to validate the different modules used in this method (see [20] for a first validation of non-rigid inter-patient matching, or [19] for tests about volume variation quantification).

To validate the dissymmetry field computation, we have performed the following experiment: starting from the 3D image I_1 of a real patient, we have simulated an artificial expansion (a mass effect) at a known location and of a known radius in the right hemisphere of the brain (image D_1). We have then computed the dissymmetry field F, $||F||$ and $||F||div(F)$ of D_1 (see figure 6), and compared it with the dissymmetry field obtained directly with I_1.

The deformation can be seen visually by comparing I_1 and D_1, but with D_1 alone, it is hard to determine visually the nature and amplitude of the deformation. In the $||F||$ images, there is a large region where the norm of the dissymmetry vectors are very high. It is therefore easy to detect that there is something unusual going on with respect to perfect symmetry, but it is however very difficult to determine the "cause" of the dissymmetry, that is the focus of expansion. This focus can be emphasized only by using a vector field operator appropriate to expansion/atrophy. In the image presenting $||F||div(F)$, the expansion translates into a roughly spherical shaped white region in the right hemisphere (on the left in the image), centered on the focus of expansion. Of course, it also translates into a symmetrical spherical dark region in the left hemisphere. The signal is less obvious in the outer boundary of the brain because it is corrupted by the natural dissymmetry of these regions. The "aperture" problem, which states that deformation are easier to detect in directions perpendicular to interfaces (such as grey/white matter) than in parallel directions explains also why perfect spherical shapes are not retrieved.

In figure 7, we present the subtraction between I_1 images and D_1 images to emphasize the effects created by the expansion only. Again, only the $||F||div(F)$ provides a clear signal with respect to the localization and extension of the expansion. We hope to be able to emphasize with this technique the effect of a growing tumor such as a glioblastoma, which is very difficult to segment because of its diffusion within the tissue.

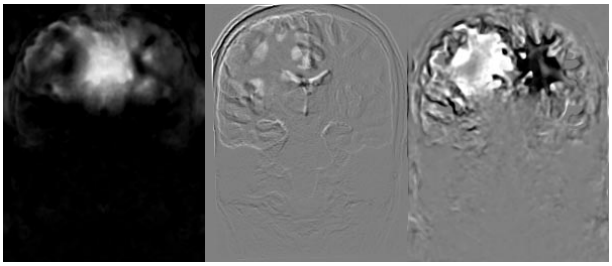

Figure 7. Subtraction of images I_1 and images D_1 to emphasize the deformation effects only.

6. Some preliminary experimental results

The following results are very preliminary. In particular, they are not validated medical studies but are presented here only to illustrate the potential applications of our method. Much more work and strong collaborations with anatomists, along with much larger image databases are needed to lead to medically significant results.

6.1. A population of healthy right handed males

A first experiment is on a population of 3D MR scans of ten different healthy subjects, all of them being right handed males. These subjects have been selected for the medical study described in [14]. Their handedness was ascertained using the Edinburgh Handedness Inventory (short form) which is a 10 item questionnaire giving a laterality quotient percentage from -100 (left handed) to 100 (right handed). Other metrics of handedness are described in [12]. The 10 subjects rated a minimum of 87 with respect to this scale. We have realigned automatically all the images with respect to the mid-plane, computed their dissymmetry maps, applied the norm-times-divergence operator and fused all the information in the frame of an eleventh subject's image (right handed rating 100) also realigned, exactly as it was described in section 4.3.1 and summarized in figure 5.

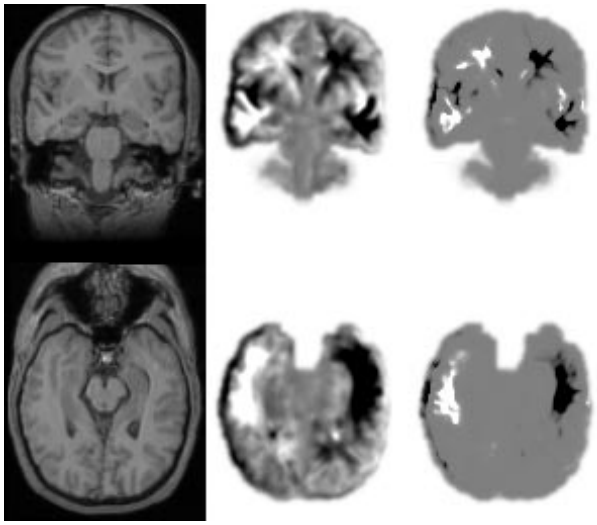

Figure 8. Significant dissymmetry for a population of 10 healthy right handed males. Left: reference patient; middle: average of the 10 $||F||div(F)||$ maps; right: significance map for $\alpha_0 = 0.001$. The right temporal lobe (on the left in the image) is indeed significantly larger than the left one for normal anatomy.

The results are presented in figure 8 for coronal and axial cross sections and at the level of the temporal lobe only. The left images present the reference subject. The images in the middle present the average of $||F||div(F)$ for the 10 subjects. The significance map (the right images) present the loci which are significantly dissymmetrical (respectively larger:white or smaller:black). We have normalized the image of the significance map with a significance level $\alpha_0 = 0.001$ (that is, pure white or pure black means $\alpha \leq 0.001$). A mask has been applied to keep only the data at the level of the reference subject's brain. This experiment confirms that the dissymmetry map presented in figure 4 for a single subject is representative of a normal dissymmetry, which means a larger right temporal lobe (on the left in the images) in normal subjects.

6.2. Left handed versus right handed

We now illustrate what was presented in section 4.3.2: the comparison of two populations. We have compared the average of 10 right handed healthy males (handedness score ≥ 87) with the average of 3 left handed healthy males (handedness score ≤ -57). The results are presented in figure 9, with the averages of $||F||div(F)||$ for the right and left handed groups (left and middle images), and the significance map normalized using the same significance level α_0 as in figure 8 (the right images).

The results appear less conclusive than for normal dissymmetry. In particular, determining discriminant features of left handed versus right handed subjects is far from being evident. A careful exploration of the 3D data and more experiments with a larger set of right and left handed subjects are probably needed to lead to definitive conclusions.

6.3. A patient with focal aphasia

We now study a patient presenting a focal aphasia. In the image of this patient (figure 10), we note an obvious dissymmetry of the ventricles [17]. The aim of this experiment is to retrieve this dissymmetry thanks to the significance map and according to the methodology presented in section 4.3.3. Figure 10 presents coronal and axial views of the focal aphasic subjects. On the left is the original image, in the middle is the $||F||div(F)$ dissymmetry map, and on the right is the significance map with respect to the population of 10 healthy right handed males, projected back on the focal aphasic's image. The obvious dissymmetry of the brain ventricles is retrieved and correctly localized in the significance map, with very high magnitude significance values (using the same significance level as in figure 8).

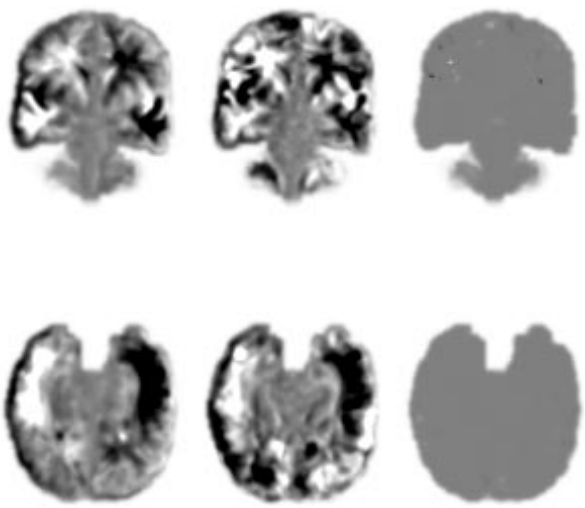

Figure 9. Dissymmetries between a population of 10 right handed males and a population of 3 left handed males. Left: average of the 10 $||F||div(F)||$ right handed maps; middle: average of 3 left handed; right: significance map for $\alpha_0 = 0.001$; the same significance level as for figure 8. These preliminary results are not conclusive with respect to a significant morphological difference between left and right handed people. Larger datasets are probably requested before drawing any conclusion.

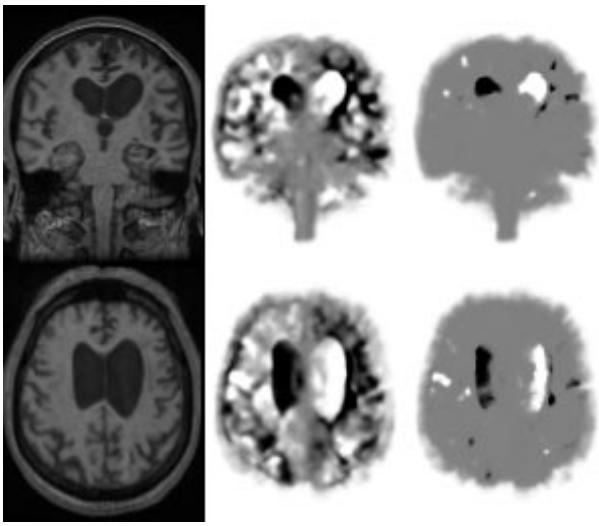

Figure 10. Significant abnormal dissymmetry of a diseased patient (focal aphasia), with respect to the population of 10 right handed normal males. Left: focal aphasic's image; middle: $||F||div(F)||$ for the aphasic; right: significance map for $\alpha_0 = 0.001$, with respect to the 10 right handed people. Note the significant dissymmetry at the level of the ventricles, which is correctly localized.

7. Conclusion

We have presented a general method to study the dissymmetry of symmetrical organs, such as the human brain, using 3D dissymmetry fields, 3D vector field operators, and the computation of 3D significance maps. The main feature of our method is that we are dealing with dense volumetric representations of the dissymmetry. We have also proposed and tested a fully automated implementation of this method, relying mainly on 3D non-rigid inter-patient matching tools applied between the images and symmetric images with respect to an arbitrary plane. A by-product of this is an unsupervised method to realign automatically symmetrical structures with respect to their mid-plane. We have also described three main application fields, which are the study of the normal dissymmetry in a given population, the comparison of the dissymmetry between two populations, and the detection of the significant abnormal dissymmetries of a patient with respect to a reference population. Finally, we have presented preliminary results for the case of human brain. These must be investigated in depth, with the careful support of anatomists and for much larger databases to enable us to draw conclusive medical results.

Acknowledgment

Many thanks to Mrs Janet Bertot for a careful proofreading of this paper. This study also relates to the EC Biomed II project BIOMORPH where we intend to use this method to study the dissymmetry of schizophrenic patients.

8. Annex

8.1. Symmetry plane computation

We want to minimize: $C = \sum_i (S(q_i) - p_i)^2$, with $S(q_i) = q_i - 2((q_i - p)^\top n)n$ and where p is a point in the symmetry plane and n the unit normal vector to the plane. By differentiating C with respect to p, we get:

$$\frac{dC}{dp} = 4 \sum_i (2p - q_i - p_i)^\top n n^\top \quad (14)$$

which demonstrates that the barycenter $G = \frac{1}{n} \sum_i \frac{(q_i + p_i)}{2}$ belongs to the symmetry plane. We get:

$$C = \sum_i (q_i - p_i)^2 + 4[(q_i - G)^\top n][(p_i - G)^\top n] \quad (15)$$

which is minimized when the following expression is minimized:

$$\sum_i n^\top [(p_i - G)(q_i - G)^\top] n \quad (16)$$

which means than n is the eigenvector associated to the smallest eigenvalue of I, where:

$$I = \sum_i (p_i - G)(q_i - G)^\top \quad (17)$$

8.2. Realignment of a 3D image

We want to demonstrate that $R^{-1/2}(I_1)$ is an image where the mid-plane is $P' : x = p_x/2$. This is equivalent to demonstrating that after the application of $R^{-1/2}$, the image $R^{-1/2}(I_1)$ and the image $R^{-1/2}(S(I_1))$ are symmetrical with respect to P', that is:

$$K \circ R^{-1/2}(I_1) = R^{-1/2} \circ S(I_1) \quad (18)$$

To demonstrate this, we shall note that S and K are planar symmetries therefore we have $K \circ K = Id$ and $S \circ S = Id$, hence:

$$R^{-1} = (S \circ K)^{-1} = K^{-1} \circ S^{-1} = K \circ S \Rightarrow K = R^{-1} \circ S \quad (19)$$

Furthermore, as $R^{-1/2}$ is an affine rotation with a rotation axis in P', $K \circ R^{-1/2}$ is also a planar symmetry, hence:

$$K \circ R^{-1/2} = (K \circ R^{-1/2})^{-1} = R^{1/2} \circ K^{-1} = R^{1/2} \circ K \quad (20)$$

Replacing K with $R^{-1} \circ S$ in equation 20 (on the right) gives the desired relation:

$$K \circ R^{-1/2} = R^{1/2} \circ R^{-1} \circ S = R^{-1/2} \circ S \quad (21)$$

References

[1] T. Anderson. *Introduction to Multivariate Statistical Analysis*. John Wiley & Sons, Inc., New York, USA, 1958.

[2] N. Ayache. *Artificial Vision for Mobile Robots: Stereo Vision and Multisensory Perception*. MIT Press, Cambridge, Massachussetts, 1991.

[3] R. Bilder, H. Wu, B. Bogerts, G. Degreef, M. Ashtari, J. Alvir, P. Snyder, and J. Lieberman. Absence of regional hemispheric volume asymmetries in first-episode schizophrenia. *American Journal of Psychiatry*, 151(10):1437–1447, October 1994.

[4] G. E. Christensen, S. C. Joshi, and M. I. Miller. Volumetric Transformation of Brain Anatomy. *IEEE Transactions on Medical Imaging*, 16(6):864–877, Dec. 1997.

[5] L. Collins, T. Peters, and A. Evans. An Automated 3D non-linear image deformation procedure for Determination of Gross Morphometric Variability in Human Brain. In R. A. Robb, editor, *VBC*, volume 2359 of *SPIE*, pages 180–190, Rochester (Minnesota) (USA), Oct. 1994.

[6] T. Crow. Schizophrenia as an anomaly of cerebral asymmetry. In K. Maurer, editor, *Imaging of the Brain in Psychiatry and Related Fields*, pages 1–17. Springer-Verlag, Berlin Heidelberg, 1993.

[7] Davatzikos, C. and Vaillant, M. and Resnick, S. and Prince, J.L. and Letovsky, S. and Bryan, R.N. Morphological Analysis of Brain Structure Using Spatial Normalization. In Höhne, K. H. and Kikinis, R., editor, *VBC*, volume 1131 of *Lecture Notes in Computer Science*, pages 355–360, Hamburg (Germany), sep 1996. Springer.

[8] R. Davidson and K. Hugdahl. *Brain Asymmetry*. A Bradford Book, 1994.

[9] L. DeLisi, M. Sakuma, M. Kushner, D. Finer, A. Hoff, and T. Crow. Anomalous cerebral asymmetry and language processing in schizophrenia. *Schizophrenia Bulletin*, 23(2):255–271, 1997.

[10] K. Friston, C. Frith, P. Liddle, R. Dolan, A. Lammertsma, and R. Frackowiak. The relationship between global and local changes in PET scans. *Journal of cerebral blood flow and metabolism*, 10:458–466, 1990.

[11] J. C. Gee, M. Reivich, and R. Bajcsy. Elastically deforming 3D atlas to match anatomical brain images. *Journal of Computer Assisted Tomography*, 17(2):225–236, March 1993.

[12] M. Holder. *Hand Preference Questionnaires: One Gets What One Asks For*. M. phil. thesis, Department of Anthropology, Rutgers University, New Brunswick, New Jersey, U.S.A., 1992. Electronic version: http://www.indiana.edu/ primate/forms/hand.html.

[13] R. Hunter, M. Jones, and F. Cooper. Modified lumbar air encephalography in the investigation of long stay psychatric patients. *J. Neurol. Sci.*, 6:593–596, 1968.

[14] C. Mackay, N. Roberts, A. Mayes, J. Downes, J. Foster, and D. Mann. An exploratory study of the relationship between face recognition memory and the volume of medial temporal lobe structures in healthy young males. *Behavioural Neurology*, 1997.

[15] F. Maes, A. Collignon, V. D., G. Marchal, and P. Suetens. Multimodality Image Registration by Maximization of Mutual Information. *IEEE Transactions on Medical Imaging*, 16(2):187–198, Apr. 1997.

[16] P. Marais, R. Guillemaud, M. Sakuma, A. Zisserman, and M. Brady. Visualising Cerebral Asymmetry. In Höhne, K.H. and Kikinis, R., editor, *Visualization in Biomedical Computing*, volume 1131 of *Lecture Notes in Computer Science*, pages 411–416, Hamburg (Germany), Sept. 1996. Springer.

[17] G. Subsol, N. Roberts, M. Doran, and J. P. Thirion. Automatic Analysis of Cerebral Atrophy. *Magnetic Resonance Imaging*, 15(8):917–927, 1997.

[18] J.-P. Thirion. Non-rigid matching using demons. In *Computer Vision and Pattern Recognition, CVPR'96*, San Francisco, California USA, June 1996. Electronic version: http://www.inria.fr/RRRT/RR-2547.html.

[19] J.-P. Thirion and G. Calmon. Measuring lesion growth from 3D medical images. In *Nonrigid and Articulated Motion Workshop (NAM'97)*, Puerto Rico, June 1997. IEEE. Electronic version : http://www.inria.fr/RRRT/RR-3101.html.

[20] J.-P. Thirion, G. Subsol, and D. Dean. Cross validation of three inter-patients matching methods. In *VBC*, volume 1131 of *Lecture Notes in Computer Science*, pages 327–336, Hamburg, Germany, September 1996.

[21] P. Thompson and A. Toga. Detection, visualisation and animation of abnormal anatomic structure with a deformable probabilistic brain atlas based on random vector field transformations. *Medical Image Analysis (MEDIA)*, 1(4):271–294, September 1997.

[22] P. Viola and W. M. I. Wells. Alignment by maximization of mutual information. In *Fifth Int. Conf. on Computer Vision, ICCV'95*, pages 16–23, Cambridge, Massachussetts, June 1995. IEEE.